



Originally published as:

Scheingross, J., Hovius, N., Dellinger, M., Hilton, R. G., Repasch, M., Sachse, D., Gröcke, D. R., Vieth-Hillebrand, A., Turowski, J. (2019): Preservation of organic carbon during active fluvial transport and particle abrasion. - *Geology*, 47, 10, pp. 958—962.

DOI: <http://doi.org/10.1130/G46442.1>

1 Preservation of organic carbon during active fluvial transport
2 and particle abrasion

3 **Joel S. Scheingross^{1,2*}, N. Hovius^{1,3}, M. Dellinger⁴, R.G. Hilton⁴, M. Repasch^{1,3}, D. Sachse¹,**
4 **D.R. Gröcke⁵, A.Vieth-Hillebrand¹, and J.M. Turowski¹**

5 *¹GFZ German Research Centre for Geosciences, Potsdam, Germany*

6 *²Dept. of Geological Sciences and Engineering, University of Nevada, Reno, USA*

7 *³Institute of Geosciences, University of Potsdam, Germany*

8 *⁴Dept. of Geography, Durham University, UK*

9 *⁵Dept. of Earth Sciences, Durham University, UK*

10 **jscheingross@unr.edu*

11 **ABSTRACT**

12 Oxidation of particulate organic carbon (POC) during fluvial transit releases CO₂ to the
13 atmosphere and can influence global climate. Field data show large POC oxidation fluxes in
14 lowland rivers; however, it is unclear if POC losses occur predominantly during in-river
15 transport, where POC is in continual motion within an aerated environment, or during transient
16 storage in floodplains, which may be anoxic. Determining the locus of POC oxidation in lowland
17 rivers is needed to develop process-based models to predict POC losses, constrain carbon
18 budgets, and unravel links between climate and erosion. However, sediment exchange between
19 rivers and floodplains makes differentiating POC oxidation during in-river transport from
20 oxidation during floodplain storage difficult. Here, we isolate in-river POC oxidation using
21 flume experiments transporting petrogenic and biospheric POC without floodplain storage. Our
22 experiments show solid phase POC losses of 0-10% over ~10³ km of fluvial transport, compared

23 to ~7% to >50% losses observed in rivers over similar distances. The production of dissolved
24 organic carbon (DOC) and dissolved rhenium (a proxy for petrogenic POC oxidation) are
25 consistent with small POC losses, and replicate experiments in static water tanks give similar
26 results. Our results show that fluvial sediment transport, particle abrasion, and turbulent mixing
27 have a minimal role on POC oxidation, and suggest that POC losses may accrue primarily in
28 floodplain storage.

29 **INTRODUCTION**

30 Fluvial transport of POC, including discrete particles and mineral-associated organic
31 matter >0.2 μm , represents the primary source of terrestrial organic carbon to the ocean (e.g.,
32 Blair and Aller, 2012; Bianchi et al., 2018). POC fate during fluvial transit affects atmospheric
33 CO_2 levels over a range of timescales (Cole et al., 2007; Galy et al., 2007). Transient storage of
34 CO_2 sequestered via photosynthesis in soils and biomass (biospheric POC, POC_{bio}), represents a
35 short-term (< 10^5 y) carbon sink (Bernier, 1999). POC_{bio} mobilized by and transported through
36 rivers can be oxidized and returned to the atmosphere as CO_2 (Richey et al., 2002; Mayorga et
37 al., 2005), or delivered to depositional basins to create a long-term (> 10^6 y) carbon sink (e.g.,
38 France-Lanord and Derry, 1997). This CO_2 sink may be offset by CO_2 released from oxidation of
39 fossilized organic carbon within sedimentary rock (petrogenic organic carbon, $\text{POC}_{\text{petro}}$) during
40 exhumation and transport (e.g., Bouchez et al., 2010).

41 POC losses during fluvial transit can be substantial. Amazon basin POC_{bio} and $\text{POC}_{\text{petro}}$
42 oxidation fluxes are approximately an order of magnitude larger than their respective fluxes to
43 the ocean (Richey et al., 2002; Bouchez et al., 2010). Similarly, ~50% of POC_{bio} and $\text{POC}_{\text{petro}}$ is
44 lost during transit across the Ganges alluvial basin (Galy et al., 2008a;b). Despite large POC loss
45 in transit, the location of POC oxidation is poorly constrained, as existing measurements cannot

46 distinguish between oxidation during in-river transport and during floodplain storage. In rivers,
47 fluid turbulence mixes and aerates water, which may enhance oxidation rates (Hartnett et al.,
48 1998), and increases in sediment specific surface area (SSA) from particle abrasion (e.g., Attal
49 and Lave, 2009) can further expose mineral-associated POC_{bio} and $\text{POC}_{\text{petro}}$ to oxidative
50 conditions, while also creating fine particles onto which discrete POC particles can attach to.
51 However, the time POC spends in river transport is small relative to floodplain storage (e.g.,
52 Torres et al., 2017). Intermittent floodplain storage may allow sufficient time for POC oxidation
53 (Arora et al., 2016; Scheingross et al., 2018; Wan et al., 2018), but POC can be subject to anoxic
54 conditions which may promote POC preservation (Boye et al., 2017). The relative rates of POC
55 oxidation during in-river transport versus floodplain storage is a key unknown which is needed to
56 develop a process-level understanding of source to sink POC transfer and oxidation.

57 Determining the location of POC oxidation in lowland basins is complicated by tributary
58 mixing (Galy et al., 2008b; Bouchez et al., 2010) and exchange of POC between rivers and
59 floodplains (Torres et al., 2017). An alternative approach is to isolate in-river POC oxidation via
60 laboratory experiments. Analog experiments have fundamentally advanced river mechanics
61 (Paola et al., 2009); however, flume experiments have yet to explore POC oxidation. Existing
62 laboratory investigations of organic carbon oxidation (e.g., Chang and Berner, 1999; Druhan et
63 al., 2014) were not designed to simulate the physical processes present in natural rivers (e.g.,
64 particle abrasion).

65 Here, we evaluate POC oxidation in flume experiments transporting carbon-rich sediment
66 without floodplain storage. Our experiments show minimal evidence for POC oxidation despite
67 $\sim 10^3$ km of fluvial transport, a distance similar to the lowland portion of the Ganges River. These
68 results are consistent with the idea that POC oxidation in lowland basins occurs primarily during

69 floodplain storage (e.g., Torres et al., 2017), such that the rate and magnitude of CO₂ evasion in
70 alluvial basins is likely set by POC residence time in aerobic floodplains.

71 **EXPERIMENTAL AND ANALYTICAL METHODS**

72 In lowland basins, water chemistry, microbial communities, and more can influence POC
73 oxidation (e.g., Battin et al., 2009; Druhan et al., 2014; Bianchi et al., 2018). Here we seek to
74 isolate the role of sediment transport, particle abrasion, and liquid-water leaching on POC
75 oxidation using annular flumes that re-circulate sediment, and static tanks (control experiments)
76 where POC is subject to liquid-water leaching without sediment transport (Fig. 1). Experiments
77 use natural sediments with native microbial communities and a 1:10 mix of de-ionized to tap
78 water with major element concentrations similar to rivers in the Gaillardet (1999) database (Fig.
79 DR1 in the Data Repository¹).

80 Turbulent, subcritical flow in flume experiments (Reynolds number $>10^4$, Froude number
81 ~ 0.2) produced dynamical scaling with natural rivers (Paola et al., 2009), with depth-averaged
82 velocities of $\sim 0.25 \pm 0.02$ m/s (Table DR1) similar to near-bed flow velocities in rivers (e.g.,
83 Smith and McLean, 1977). Visual observations in a transparent flume showed continual motion
84 of sediment without static deposits. Experiments ran 6-8 weeks at room temperature, producing
85 suspended sediment transport distances of ~ 900 - 1200 km (see the Data Repository; Table DR2).

86 We performed nine experiments with four distinct materials (Table DR2). To explore the
87 role of crystallographic order on POC_{petro} oxidation, we used lignite and shale containing
88 relatively amorphous and more crystalline carbon, respectively, collected from outcrop. To
89 explore POC_{bio} oxidation, we collected sediment from a headwater stream underlain by volcanic
90 rock (Smith and Roe, 2015) with well-described POC composition (Lookout Creek, Oregon
91 (Smith, 2013)) and a lowland river with negligible POC_{petro} quantities (Rio Bermejo, Argentina)

92 where preliminary data shows significant POC oxidation during floodplain storage (Scheingross
 93 et al., 2018). In select experiments, we varied sediment size to examine the role of sediment
 94 abrasion on POC oxidation (see the Data Repository). Blank experiments (without sediment and
 95 transporting combusted quartz sand) showed no systematic changes in DOC and returned POC
 96 concentrations below measurement detection limit (Table DR3, Fig. DR2).

97 We assessed solid and dissolved load changes with sediment samples at the start and end
 98 of experiments and 5-10 water samples per experiment (see the Data Repository). Solid samples
 99 were analyzed for POC content (C_{org} , wt.%) and stable carbon isotopes ($\delta^{13}C_{org}$, ‰) following
 100 carbonate removal using an EA-IRMS. Particle size distribution was analyzed using a laser
 101 diffraction particle size analyzer or via optical images. We analyzed water samples for DOC
 102 concentration using liquid-chromatography organic carbon detection, major ions by ion
 103 chromatography and ICP-OES, and dissolved rhenium concentration, a POC_{petro} oxidation proxy
 104 (Dalai et al., 2002; Jaffe et al., 2002; Hilton et al., 2014), using ICP-MS (see the Data
 105 Repository).

106 **EVALUATING POC OXIDATION**

107 POC loss during fluvial transit includes direct CO_2 and DOC production. We assume any
 108 organic carbon loss from the solid phase represents long-term POC oxidation because terrestrial
 109 DOC is rapidly oxidized in the ocean (Bianchi, 2011). We quantify POC oxidation by measuring
 110 the percent change in POC mass over an experiment

$$111 \quad \Delta M_c = \left[\left(M_{c_final} - M_{c_initial} \right) / M_{c_initial} \right] \times 100 , \quad (1)$$

112 where $M_{c_initial}$ and M_{c_final} are the solid POC mass at the experiment start and end, respectively
 113 (see the Data Repository). Solid load POC loss yields negative ΔM_c .

114 DOC measurements provide additional POC loss constraints. We measure the percentage
 115 mass fraction, f , of organic carbon transferred from the solid to the dissolved load as

$$116 \quad f_{DOC} = \left(M_{DOC_max} / M_{c_initial} \right) \times 100, \quad (2)$$

117 where M_{DOC_max} is the maximum DOC mass in the experiment (see the Data Repository). Using
 118 M_{DOC_max} gives an upper limit on f_{DOC} ; however, f_{DOC} is a minimum constraint on total POC loss
 119 because DOC can be oxidized during the experiment.

120 Rhenium is typically associated with organic matter in sedimentary rocks and upon
 121 oxidation forms a soluble anion within the dissolved load, thus POC_{petro} oxidation during the
 122 experiment could result in increased dissolved rhenium concentrations (Hilton et al., 2014). We
 123 express the mass of rhenium transferred from the solid to dissolved load as

$$124 \quad f_{Re} = \left(M_{diss_Re} / M_{Re_initial} \right) \times 100, \quad (3)$$

125 where M_{diss_Re} is the accumulated dissolved rhenium mass during the experiment and $M_{Re_initial}$ is
 126 the initial rhenium mass in the sediment (see the Data Repository). For M_{diss_Re} , we exclude an
 127 initial rapid period of change of ion concentrations (Re , SO_4^{2-} and Ca^{2+}) which is inconsistent
 128 with the lowland river processes we seek to model (see the Data Repository). f_{Re} provides a
 129 maximum constraint on POC_{petro} loss due to contributions of dissolved rhenium from non-
 130 POC_{petro} phases (Horan et al., In Press).

131 **EXPERIMENTAL RESULTS**

132 POC loss in all runs was small relative to measurement uncertainty. ΔM_c never fell below
 133 $-10.1 \pm 4.1\%$ and $-9.4 \pm 4.1\%$ in POC_{petro} and POC_{bio} experiments, respectively, and the majority of
 134 experiments showed no POC loss (ΔM_c greater than or within error of 0%, Fig. 2B). $\Delta M_c > 0\%$
 135 (POC gain) is likely due to solid sample heterogeneity. Shifts in $\delta^{13}C_{org}$ values were typically

136 within analytical uncertainty, suggesting that POC stable isotope composition stayed constant
137 during sediment transport (Fig. 2C).

138 DOC production was small; f_{DOC} never exceeded 0.6% and 5.3% in the POC_{petro} and
139 POC_{bio} experiments, respectively (Fig. 2D). For POC_{petro} experiments, after some initial water-
140 sediment interactions over <1 d, shale experiments showed negligible DOC production relative
141 to the background levels, while the lignite flume experiment showed steady DOC decrease (Fig.
142 DR3, Table DR4). The POC_{bio} experiments showed a sharp DOC increase during the first 24 h,
143 and then slowed (Fig. DR3).

144 In the POC_{petro} experiments, dissolved ion concentrations increased rapidly over the first
145 1-4 d and then slowed (Fig. DR4). We attribute this to ion-exchange (Sayles and Mangelsdorf,
146 1979), leaching of ions from freshly exposed defect sites (White and Brantley, 2003), and/or
147 rapid carbonate dissolution (Chou et al., 1989) forced by the interaction of fresh rock with a fluid
148 out of equilibrium with the sediment. Accounting for this (see the Data Repository) yields f_{Re}
149 values that vary from <0% to $14 \pm 3\%$ (Fig. 2E). These changes tend to be within error of or
150 greater than ΔM_c values, consistent with f_{Re} as an upper limit on POC_{petro} losses.

151 Flume experiments show no systematic difference in ΔM_c , f_{DOC} , and f_{Re} compared to their
152 associated control run (Fig. 2). For cases with initial median grain diameter (D_{50}) >500 μm
153 fluvial transport caused particle abrasion in flume experiments (Fig. 2A), yet flume and
154 (abrasion-free) control ΔM_c and f_{Re} values were within error of each other or indicated increased
155 oxidation in the control run, suggesting a minimal influence of particle abrasion on POC loss
156 (Fig. 2B and E). Experiments with D_{50} <500 μm showed no detectable abrasion, likely due to
157 viscous damping of particle impacts (Joseph et al., 2001) (Table DR2).

158 **POTENTIAL FOR POC OXIDATION DURING IN-RIVER TRANSPORT**

159 The lack of systematic differences between the flume and control experiments suggests
160 an insignificant role of sediment transport and particle abrasion in POC oxidation relative to
161 liquid-water leaching. The largest POC mass losses ($-8\% < \Delta M_c < -10\%$) occurred for $D_{50} > 125 \mu\text{m}$
162 (Fig. 2), suggesting that POC oxidation rates may be more strongly influenced by whether and
163 how carbon is bound to sediment, rather than by sediment transport processes or size (a proxy for
164 particle SSA) (Blair and Aller, 2012).

165 The maximum $\text{POC}_{\text{petro}}$ losses measured in our experiments ($\Delta M_c = -10 \pm 4\%$ and the proxy
166 $f_{\text{Re}} = 14 \pm 3\%$, Fig. 2) were small compared to field measurements in lowland river systems.
167 Reported $\text{POC}_{\text{petro}}$ losses between the mountain front and coastline in the Amazon and Ganges
168 rivers range from 7-50% per 10^3 km (see the Data Repository); up to ~5 times larger than the
169 maximum $\text{POC}_{\text{petro}}$ loss in our experiments (Fig. 2). These losses occur despite the prevalence of
170 graphitized $\text{POC}_{\text{petro}}$ in the Ganges, which is likely more resistant to oxidation than the
171 disordered lignite used here (Galy et al., 2008a).

172 Experimental POC_{bio} losses were up to $\Delta M_c = -9 \pm 4\%$. Unlike $\text{POC}_{\text{petro}}$, which is typically
173 sourced from bedrock in river headwaters, POC_{bio} is sourced from vegetation and soils along the
174 entire river length. The Amazon (Mayorga et al., 2005; Aufdenkampe et al., 2007) and Ganges
175 (Galy et al., 2008b) basins show replacement of headwater-derived POC with floodplain POC_{bio} .
176 Galy et al. (2008b) suggest $>50\%$ replacement of POC_{bio} over ~900 km of fluvial transit along
177 the Ganges, ~5 times greater than the maximum loss in our experiments. We interpret the lack of
178 large differences between flume and control experiments and consistently low POC losses
179 indicated by multiple measurements (ΔM_c , f_{DOC} , and the proxy f_{Re}) to suggest that the physical
180 processes in river systems, i.e., turbulent fluid mixing, sediment transport, and particle abrasion,

181 cannot produce the magnitude of POC oxidation observed over equivalent transport distances in
182 river systems.

183 **IS POC OXIDIZED DURING IN-RIVER TRANSPORT OR FLOODPLAIN STORAGE?**

184 Despite field measurements showing large POC losses in lowland rivers (Richey et al.,
185 2002; Galy et al., 2008a;b; Bouchez et al., 2010), it remains unknown whether POC oxidation
186 occurs primarily during active river transport or transient floodplain storage. In nine laboratory
187 experiments, we observed no significant influence of $\sim 10^3$ km sediment transport on POC
188 oxidation. POC mass loss never exceeded $\Delta M_c = -10\%$, and 6 of 9 experiments showed POC loss
189 within error of zero or POC gain, compared to field observations of 7% to >50% POC loss over
190 equivalent transport distances. Chemical and biological processes not systematically explored in
191 our experiments may increase POC oxidation during in-river transport (e.g., Battin et al., 2009;
192 Druhan et al., 2014) and are ripe for future experimental study. However, by using sediment with
193 native microbial communities and water similar in chemical composition to major rivers, our
194 results suggest that POC oxidation in lowland rivers occurs primarily during floodplain storage
195 rather than during in-river transport. POC oxidation is likely sensitive to the residence time of
196 sediment in floodplains, as well as the rate and depth of burial, local redox conditions, and
197 microbial dynamics, variables that should be systematically explored in future experiments and
198 fieldwork to build mechanistic models of POC transport and oxidation.

199 **ACKNOWLEDGEMENTS**

200 We thank Ralf Kühner, Annette Schmid-Röhl, and Kirsten Cook for assistance in sample
201 collection and Markus Reich for flume design. Johannes Glodny, Nina Golombek, Kristin
202 Günther, Hima Hassenruck-Gudipati, Petra Meier, Sylvia Pinkerneil, Birgit Plessen, Toni
203 Schmidt, Martin West and Carolin Zorn assisted with experiments, sample preparation, and
204 measurements. Grain size, surface area, and ICP-OES measurements were made at the GFZ Sed
205 Lab Helmholtz Laboratory for the Geochemistry of the Earth Surface at GFZ Potsdam,
206 respectively; Liane Benning facilitated surface area measurements. We thank Mark Torres and
207 Maarten Lupker for discussion, and Brad Rosenheim and three anonymous referees for reviews.
208 We acknowledge support from an Alexander von Humboldt Postdoctoral Fellowship (JSS), a

209 European Research Council Starting Grant (ERC-StG, 678779, ROC-CO₂ to RGH), and a
210 COFUND Durham University Junior Research Fellowship (MD).
211

212 REFERENCES

- 213 Arora, B., Spycher, N. F., Steefel, C. I., Molins, S., Bill, M., Conrad, M. E., Dong, W. M.,
214 Faybishenko, B., Tokunaga, T. K., Wan, J. M., Williams, K. H., and Yabusaki, S. B.,
215 2016, Influence of hydrological, biogeochemical and temperature transients on
216 subsurface carbon fluxes in a flood plain environment: *Biogeochemistry*, v. 127, no. 2-3,
217 p. 367-396.
- 218 Attal, M., and Lave, J., 2009, Pebble abrasion during fluvial transport: Experimental results and
219 implications for the evolution of the sediment load along rivers: *Journal of Geophysical*
220 *Research-Earth Surface*, v. 114.
- 221 Aufdenkampe, A. K., Mayorga, E., Hedges, J. I., Llerena, C., Quay, P. D., Gudeman, J.,
222 Krusche, A. V., and Richey, J. E., 2007, Organic matter in the Peruvian headwaters of the
223 Amazon: Compositional evolution from the Andes to the lowland Amazon mainstem:
224 *Organic Geochemistry*, v. 38, no. 3, p. 337-364.
- 225 Battin, T. J., Kaplan, L. A., Findlay, S., Hopkinson, C. S., Marti, E., Packman, A. I., Newbold, J.
226 D., and Sabater, F., 2009, Biophysical controls on organic carbon fluxes in fluvial
227 networks (vol 1, pg 95, 2008): *Nature Geoscience*, v. 2, no. 8, p. 595-595.
- 228 Berner, R. A., 1999, A new look at the long-term carbon cycle: *GSA Today*, v. 9, no. 11.
- 229 Bianchi, T. S., 2011, The role of terrestrially derived organic carbon in the coastal ocean: A
230 changing paradigm and the priming effect: *Proceedings of the National Academy of*
231 *Sciences of the United States of America*, v. 108, no. 49, p. 19473-19481.
- 232 Bianchi, T. S., Cui, X., Blair, N. E., Burdige, D. J., Eglinton, T. I., and Galy, V., 2018, Centers of
233 organic carbon burial and oxidation at the land-ocean interface: *Organic Geochemistry*, v.
234 115, p. 138-155.
- 235 Blair, N. E., and Aller, R. C., 2012, The Fate of Terrestrial Organic Carbon in the Marine
236 Environment: *Annual Review of Marine Science*, Vol 4, v. 4, p. 401-423.
- 237 Bouchez, J., Beyssac, O., Galy, V., Gaillardet, J., France-Lanord, C., Maurice, L., and Moreira-
238 Turcq, P., 2010, Oxidation of petrogenic organic carbon in the Amazon floodplain as a
239 source of atmospheric CO₂: *Geology*, v. 38, no. 3, p. 255-258.
- 240 Boye, K., Noël, V., Tfaily, M. M., Bone, S. E., Williams, K. H., Bargar, John R., and Fendorf,
241 S., 2017, Thermodynamically controlled preservation of organic carbon in floodplains:
242 *Nature Geoscience*, v. 10, no. 6, p. 415-419.
- 243 Chang, S. B., and Berner, R. A., 1999, Coal weathering and the geochemical carbon cycle:
244 *Geochimica Et Cosmochimica Acta*, v. 63, no. 19-20, p. 3301-3310.
- 245 Chou, L., Garrels, R. M., and Wollast, R., 1989, Comparative study of the kinetics and
246 mechanisms of dissolution of carbonate minerals: *Chemical Geology*, v. 78, p. 269-282.
- 247 Cole, J. J., Prairie, Y. T., Caraco, N. F., McDowell, W. H., Tranvik, L. J., Striegl, R. G., Duarte,
248 C. M., Kortelainen, P., Downing, J. A., Middelburg, J. J., and Melack, J., 2007, Plumbing
249 the global carbon cycle: Integrating inland waters into the terrestrial carbon budget:
250 *Ecosystems*, v. 10, no. 1, p. 171-184.
- 251 Dalai, T. K., Singh, S. K., Trivedi, J. R., and Krishnaswami, S., 2002, Dissolved rhenium in the
252 Yamuna River System and the Ganga in the Himalaya: Role of black shale weathering on

- 253 the budgets of Re, Os, and U in rivers and CO₂ in the atmosphere: *Geochimica Et*
254 *Cosmochimica Acta*, v. 66, no. 1, p. 29-43.
- 255 Druhan, J. L., Bill, M., Lim, H., Wu, C., Conrad, M. E., Williams, K. H., DePaolo, D. J., and
256 Brodie, E. L., 2014, A large column analog experiment of stable isotope variations during
257 reactive transport: II. Carbon mass balance, microbial community structure and
258 predation: *Geochimica Et Cosmochimica Acta*, v. 124, p. 394-409.
- 259 France-Lanord, C., and Derry, L. A., 1997, Organic carbon burial forcing of the carbon cycle
260 from Himalayan erosion: *Nature*, v. 390, no. 6655, p. 65-67.
- 261 Gaillardet, J., Dupre, B., and Allegre, C. J., 1999, Geochemistry of large river suspended
262 sediments: Silicate weathering or recycling tracer?: *Geochimica Et Cosmochimica Acta*,
263 v. 63, no. 23-24, p. 4037-4051.
- 264 Galy, V., Beyssac, O., France-Lanord, C., and Eglinton, T., 2008a, Recycling of Graphite During
265 Himalayan Erosion: A Geological Stabilization of Carbon in the Crust: *Science*, v. 322,
266 no. 5903, p. 943-945.
- 267 Galy, V., France-Lanord, C., Beyssac, O., Faure, P., Kudrass, H., and Palhol, F., 2007, Efficient
268 organic carbon burial in the Bengal fan sustained by the Himalayan erosional system:
269 *Nature*, v. 450, no. 7168, p. 407-U406.
- 270 Galy, V., France-Lanord, C., and Lartiges, B., 2008b, Loading and fate of particulate organic
271 carbon from the Himalaya to the Ganga-Brahmaputra delta: *Geochimica Et*
272 *Cosmochimica Acta*, v. 72, no. 7, p. 1767-1787.
- 273 Hartnett, H. E., Keil, R. G., Hedges, J. I., and Devol, A. H., 1998, Influence of oxygen exposure
274 time on organic carbon preservation in continental margin sediments: *Nature*, v. 391, no.
275 6667, p. 572-574.
- 276 Hilton, R. G., Gaillardet, J., Calmels, D., and Birck, J., 2014, Geological respiration of a
277 mountain belt revealed by the trace element rhenium: *Earth and Planetary Science*
278 *Letters*, v. 403, p. 27-36.
- 279 Horan, K., Hilton, R. G., Dellinger, M., Tipper, E., Galy, V., Calmels, D., Selby, J., Gaillardet,
280 J., Ottley, C. J., Parsons, D. R., and Burton, K. W., In Press, Carbon dioxide emissions by
281 rock organic carbon oxidation and the net geochemical carbon budget of the Mackenzie
282 River Basin: *American Journal of Science*.
- 283 Jaffe, L. A., Peucker-Ehrenbrink, B., and Petsch, S. T., 2002, Mobility of rhenium, platinum
284 group elements and organic carbon during black shale weathering: *Earth and Planetary*
285 *Science Letters*, v. 198, no. 3-4, p. 339-353.
- 286 Joseph, G. G., Zenit, R., Hunt, M. L., and Rosenwinkel, A. M., 2001, Particle-wall collisions in a
287 viscous fluid: *Journal of Fluid Mechanics*, v. 433, p. 329-346.
- 288 Mayorga, E., Aufdenkampe, A. K., Masiello, C. A., Krusche, A. V., Hedges, J. I., Quay, P. D.,
289 Richey, J. E., and Brown, T. A., 2005, Young organic matter as a source of carbon
290 dioxide outgassing from Amazonian rivers: *Nature*, v. 436, no. 7050, p. 538-541.
- 291 Paola, C., Straub, K., Mohrig, D., and Reinhardt, L., 2009, The "unreasonable effectiveness" of
292 stratigraphic and geomorphic experiments: *Earth-Science Reviews*, v. 97, no. 1-4, p. 1-
293 43.
- 294 Richey, J. E., Melack, J. M., Aufdenkampe, A. K., Ballester, V. M., and Hess, L. L., 2002,
295 Outgassing from Amazonian rivers and wetlands as a large tropical source of atmospheric
296 CO₂: *Nature*, v. 416, no. 6881, p. 617-620.

- 297 Sayles, F. L., and Mangelsdorf, P. C., 1979, Cation-Exchange Characteristics of Amazon River
 298 Suspended Sediment and Its Reaction with Seawater: *Geochimica Et Cosmochimica*
 299 *Acta*, v. 43, no. 5, p. 767-779.
- 300 Scheingross, J. S., Repasch, M., Hovius, N., Sachse, D., Dellinger, M., Lupker, M., Hilton, R.
 301 G., Eglinton, T., Grocke, D., Golombek, N., and Orfeo, O., 2018, The fate of organic
 302 carbon during lowland river transport and transient floodplain storage: AGU Fall Meeting
 303 abstract V11E-0070.
- 304 Smith, J. C., 2013, Particulate organic carbon mobilisation and export from temperate forested
 305 uplands [PhD: University of Cambridge].
- 306 Smith, J. D., and McLean, S. R., 1977, Spatially averaged flow over a wavy surface: *Journal of*
 307 *Geophysical Research-Oceans and Atmospheres*, v. 82, no. 12, p. 1735-1746.
- 308 Smith, R. L., and Roe, W. P., 2015, Oregon Geologic Data Compilation, release 6: State of
 309 Oregon Department of Geology and Mineral Industries,
 310 <https://www.oregongeology.org/pubs/dds/p-OGDC-6.htm>.
- 311 Torres, M. A., Limaye, A. B., Ganti, V., Lamb, M. P., West, A. J., and Fischer, W. W., 2017,
 312 Model predictions of long-lived storage of organic carbon in river deposits: *Earth Surface*
 313 *Dynamics*, v. 5, no. 4, p. 711-730.
- 314 Wan, J. M., Tokunaga, T. K., Dong, W. M., Williams, K. H., Kim, Y., Conrad, M. E., Bill, M.,
 315 Riley, W. J., and Hubbard, S. S., 2018, Deep Unsaturated Zone Contributions to Carbon
 316 Cycling in Semiarid Environments: *Journal of Geophysical Research-Biogeosciences*, v.
 317 123, no. 9, p. 3045-3054.
- 318 White, A. F., and Brantley, S. L., 2003, The effect of time on the weathering of silicate minerals:
 319 why do weathering rates differ in the laboratory and field?: *Chemical Geology*, v. 202,
 320 no. 3-4, p. 479-506.

323 **FIGURE CAPTIONS:**

324 **Figure 1:** Schematic of stainless steel flumes with (A) and without (B) paddle wheel visible. (C)
 325 Acrylic, but otherwise identical, flume used to monitor hydrodynamics with visible sediment
 326 transport.

327

328 **Figure 2:** Comparison of changes in (A) median grain size ($\Delta D_{50} = [(D_{50_final} -$
 329 $D_{50_initial})/D_{50_initial}] \times 100$, where D_{50_final} and $D_{50_initial}$ are the median grain sizes at the start and
 330 end of the experiments, respectively), (B) solid load POC (ΔM_c , Eq. 1), (C) $\delta^{13}C_{org}$, (D) DOC
 331 (f_{DOC} , Eq. 2), and (E) dissolved rhenium (f_{Re} , Eq. 3). Black squares and gray circles distinguish
 332 between the flume experiments with sediment transport and the static control tanks, respectively.

333 Gray bars and black arrow in panel (B) show field estimates for POC oxidation over ~1000 km
334 transport in the Amazon and Ganges rivers (see the Data Repository for details). $\delta^{13}\text{C}_{\text{org_initial}}$ and
335 $\delta^{13}\text{C}_{\text{org_final}}$ are the $\delta^{13}\text{C}_{\text{org}}$ values at the start and end of the experiments, respectively. Negative
336 ΔD_{50} values indicate particle abrasion and reduced ΔD_{50} uncertainty for Experiments 6 and 14 is
337 due to use of optical measurements permissible on larger grain sizes (see the Data Repository).
338 Errorbars represent propagated uncertainty of measurements as reported in the Data Repository
339 and are smaller than symbols where not shown.

340 ¹GSA Data Repository item 201Xxxx, containing additional details on methods and analysis,
341 five figures, and six tables with all experimental data, is available online at
342 www.geosociety.org/pubs/ft20XX.htm, or on request from editing@geosociety.org or
343 Documents Secretary, GSA, P.O. Box 9140, Boulder, CO 80301, USA.

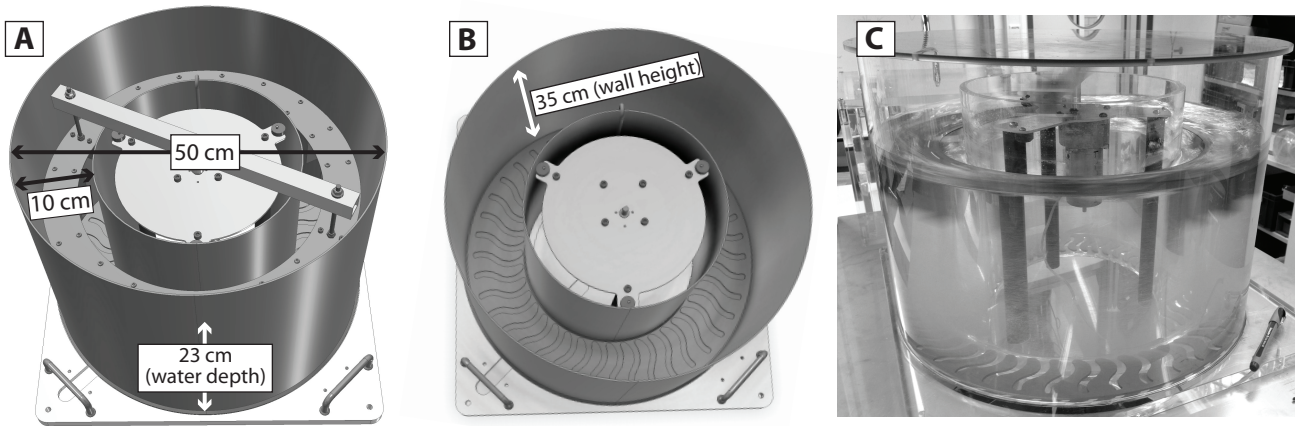


Figure 1: Schematic of stainless steel flumes with (A) and without (B) paddle wheel visible. (C) Acrylic, but otherwise identical, flume used to monitor hydrodynamics with visible sediment transport.

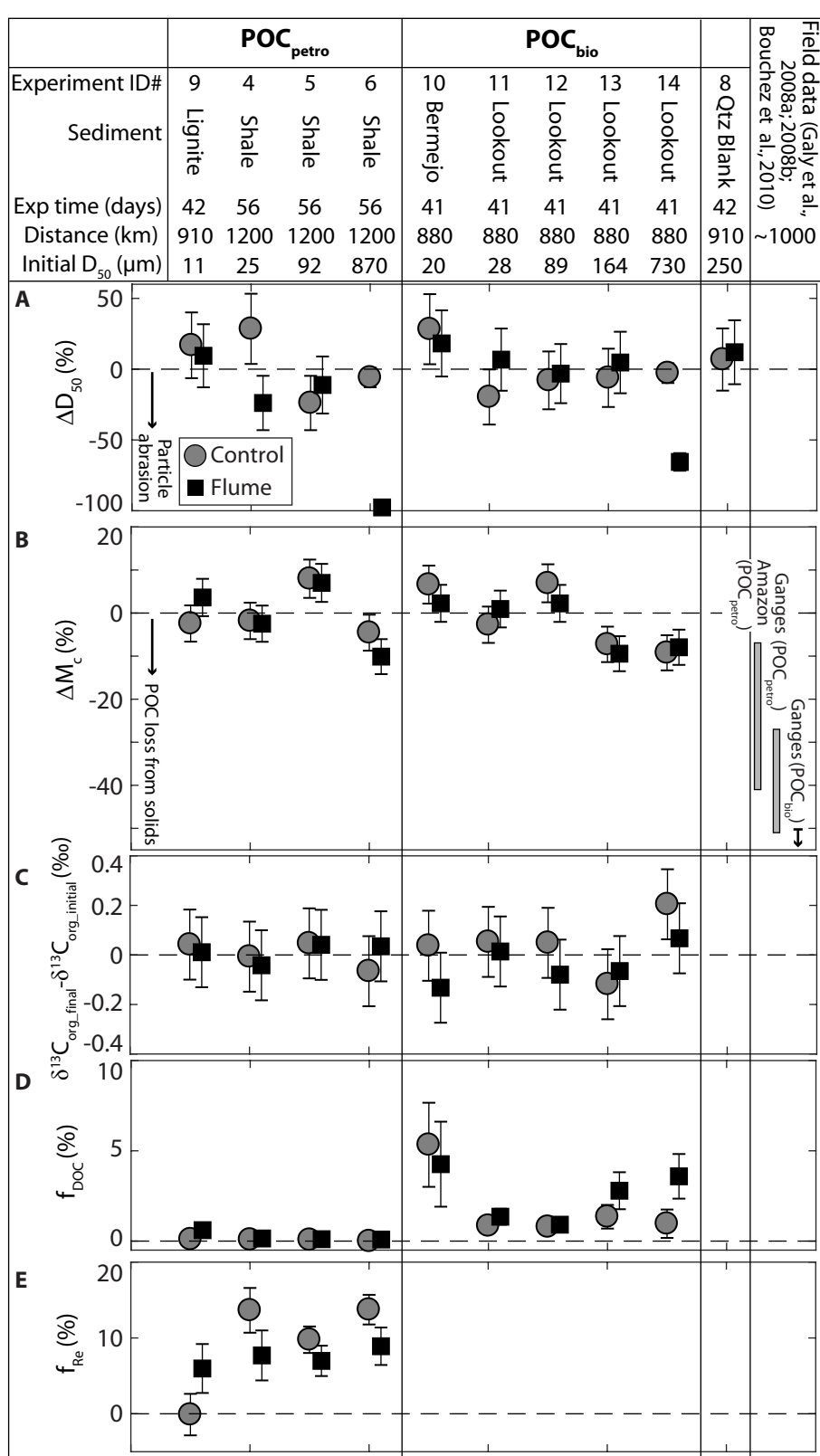


Figure 2: Comparison of changes in (A) median grain size ($\Delta D_{50} = [(D_{50_final} - D_{50_initial})/D_{50_initial}] \times 100$, where D_{50_final} and $D_{50_initial}$ are the median grain sizes at the start and end of the experiments, respectively), (B) solid load POC (ΔM_c , Eq. 1), (C) $\delta^{13}C_{org}$, (D) DOC (f_{DOC} , Eq. 2), and (E) dissolved rhenium (f_{Re} , Eq. 3). Gray bars and black arrow in panel (B) show field estimates for POC oxidation over ~ 1000 km transport in the Amazon and Ganges rivers (see the Data Repository for details). $\delta^{13}C_{org_initial}$ and $\delta^{13}C_{org_final}$ are the $\delta^{13}C_{org}$ values at the start and end of the experiments, respectively. Reduced ΔD_{50} uncertainty for Experiments 6 and 14 is due to use of optical measurements permissible on larger grain sizes (see the Data Repository). Errorbars represent propagated uncertainty of measurements as reported in the Data Repository and are smaller than symbols where not shown.

GSA Data Repository 2019XXX

Preservation of organic carbon during active fluvial transport and particle abrasion

Joel S. Scheingross^{1,2*}, N. Hovius^{1,3}, M. Dellinger⁴, R.G. Hilton⁴, M. Repasch^{1,3}, D. Sachse¹, D.R. Gröcke⁵, A.Vieth-Hillebrand¹, and J.M. Turowski¹

¹GFZ German Research Centre for Geosciences, Potsdam, Germany

²Dept. of Geological Sciences and Engineering, University of Nevada, Reno, USA

³Institute of Geosciences, University of Potsdam, Germany

⁴Dept. of Geography, Durham University, UK

⁵Dept. of Earth Sciences, Durham University, UK

*jscheingross@unr.edu

Data Repository Text

1. Additional experimental materials and methods

We used stainless steel flume and control tanks to minimize contamination from organic material. Flumes were annular (35 cm tall with 25 and 15 cm outer and inner radii, respectively) while control tanks were cylindrical (25 cm tall by 33 cm in diameter). In flumes, hydraulic roughness was provided by placing a removable, 3.2 mm thick stainless steel sheet cut into a wave pattern on the flume floor (Figure 1B). All experiments began with ~20-30 h of clear water flow before adding sediment, this allowed assessment of contamination from flume and control tanks via monitoring changes in the dissolved load. To ensure a well-mixed system, control experiments were hand-stirred for ~10 seconds, ~5 times per week. Flume and control experiments used 29.3 ± 0.4 and 16.0 ± 0.2 L of water, respectively (Table DR2). We measured water loss due to evaporation and sampling via point gage measurements of the flume and control water levels at the start and end of each experiment, using the difference between measurements and the tank geometry to estimate the total water volume loss (Table DR2).

2. Flow velocity and sediment transport

In our flume experiments, flow was driven by rotating paddles that spun at 58 ± 2.5 revolutions per minute (RPM). We measured downstream flow velocity in the flumes using an OTT C2 propeller-style flow meter placed in the center of the channel and oriented perpendicular to the main flow direction (Table DR1). All flow measurements were made in triplicate and averaged over 60 s. Depth-averaged flow velocities, U_{fluid} , for conditions in our experiment ranged from 0.24 to 0.26 m/s (Table DR1), and we use a flow velocity of 0.25 m/s for all sediment transport calculations.

We make separate estimates of particle transport distance for suspended sediment and bedload. In the downstream direction, suspended sediment is transported at the fluid velocity (McLean, 1992; Garcia, 2008), such that the suspended sediment transport distance, x_{susp} , can be approximated as

$$x_{susp} = U_{fluid}t, \quad (\text{DR1})$$

where t is time. Data compilations show bedload saltation velocity tends to be ~60-80% of the fluid velocity (Chatanantavet et al., 2013); we estimate bedload transport distance, $x_{bedload}$, as

$$x_{bedload} = 0.7x_{susp} \quad . \quad (DR2)$$

We mark the transition from bedload to suspended load transport using the ratio between fluid shear velocity, u_* (a proxy for fluid turbulence), and still water particle terminal settling velocity, w_s . Estimates for the onset of suspension vary range for $u_*/w_s > 0.2 - 2$ (Chanson, 2004), and $u_*/w_s > 1$ is often used as an order of magnitude estimate (Bagnold, 1966). We estimate particle settling velocity following Dietrich (1982), and estimate shear velocity by rearranging a standard channel flow resistance equation (Garcia, 2008)

$$u_* = \frac{U}{8.1(H / k_s)^{1/6}} \quad , \quad (DR3)$$

where $H = 23$ cm is the flume flow depth and k_s is a roughness length scale which we set equal to the 3.2 mm relief of the wave-cut sheet placed on the flume floor. Following this analysis, the threshold for suspension occurs for grains finer than ~ 160 μm diameter, resulting in sediment transport primarily in suspension for all but two of our main experiments (Table DR2).

3. Sediment collection and preparation prior to experiments

We collected Jurassic Posidonia shale and Miocene Lusatian lignite from fresh outcrops exposed at open-pit mines near Dotternhausen, Germany and Cottbus, Germany, respectively (Schreck and Glasser, 1998; Rohl et al., 2001). Sediment from Lookout Creek, USA (Smith, 2013) and Rio Bermejo, Argentina (Scheingross et al., 2018) was collected with a clean trowel from channel deposits exposed during low flow. Visual observation showed Lookout Creek and Rio Bermejo samples included fragments of leaf litter and other discrete organic particles. These samples are likely to also have mineral-associated biospheric organic matter due to the presence of fine grains, but we made no effort to distinguish if and how organic matter was bound to sediment, instead focusing on the bulk POC behavior.

All samples were oven-dried at temperatures between 40-60 °C upon return to the lab. After drying, we crushed lignite and shale samples, wet-sieved samples to distinct grain size fractions, re-oven dried sediment, and introduced sediment into the experiments. Sieving of sediments into different size fractions allowed examination of the role of particle abrasion. Larger grain sizes have higher kinetic energy of impact, producing more abrasion (Sklar and Dietrich, 2004), while grains with less than ~ 200 μm diameter in our experiment had viscous damping of impacts, limiting abrasion (Joseph et al., 2001; Scheingross et al., 2014).

4. Sample collection, processing and analytical techniques

Our water and sediment sampling frequency represents a tradeoff between high frequency measurements and limiting disturbance to the experiment. We chose water sampling frequency based on preliminary measurements from our pilot experiments (Data Repository Section 9) in order to capture major trends while minimizing the total water extracted, and limited sediment sampling to only before and after the experiment in order to obtain large sample volumes without the need to drain water from the experiments.

We used a high-density polyethylene (HDPE) syringe rinsed in de-ionized water to collect water samples from the surface of the flume and control tanks for analysis, and filtered water with single-use 0.22 μm polyethersulphone (PES) filters. At the time of water sampling, we measured pH, conductivity, dissolved oxygen, and water temperature in both flume and

control tanks with a multiprobe (Table DR5). We stored samples for DOC analysis in combusted glass vials and all other samples in HDPE bottles triple-rinsed with de-ionized water. Samples for rhenium and cation analysis were acidified with 32% nitric acid immediately after sample collection. All water samples were refrigerated from the time of collection until sample analysis.

We measured DOC concentration by liquid-chromatography organic carbon detection (LC-OCD). Phosphate buffer (pH 6.85; 2.5 g KH_2PO_4 , 1.5 g Na_2HPO_4) was used as mobile phase with a flow of 1.1 ml/min. Quantification of DOC was done by IR-detection of released CO_2 after UV photooxidation ($\lambda = 185$ nm) in a Gräntzel thin-film reactor. Replicate measurements of DOC consistently yielded error less than 25% of the measurement value (Figure DR3 and Table DR4) and we conservatively apply an error of 25% to all measurements, and propagate this 25% error in f_{DOC} calculations (Eq. 2).

Cations were measured with a Varian 720 inductively coupled plasma optical emission spectrometer (ICP-OES) at the Helmholtz Laboratory for the Geochemistry of the Earth Surface at GFZ Potsdam following Schuessler et al. (2016) (Table DR6). We used SLRS-5 (Saint-Laurent River Surface, National Research Council - Conseil National de Recherches Canada) and USGS M212 and T187 as external standards and measured an internal standard (GFZ-RW1) every 10 samples to correct for instrument drift. We report measurement error based on calibration uncertainties (Table DR7). We used a Dionex ICS1100 Ion Chromatograph to measure anion concentrations, using USGS standards M206, M208, and M212 as external standards and for quality control, we report standard deviation of triplicate measurements as an assessment of sample uncertainty (Tables DR6 and DR7). We used the inorganic dissolved data to estimate HCO_3^- using a charge balance (excluding Si), and summed all anions and cations to estimate total dissolved solids (TDS). Propagating uncertainties gives TDS error of 2-7% (Table DR7).

Dissolved rhenium concentration was determined by direct calibration against a set of seven standards with varying Re abundances and similar matrixes to river water, using quadrupole inductively coupled plasma mass spectrometry (Q-ICP-MS, Agilent Technologies 7900). Standards and samples were doped with a known concentration of internal standard Tb and Bi to correct for instrumental drift. Accuracy and precision of the measurements was assessed by repeated measurements of riverine standard reference materials SLRS-5 and SLRS-6. The standards confirmed better than 5% accuracy and precision, and we propagate 5% uncertainty from these measurements in calculations of f_{Re} (Eq. 3).

Total water collection for sample analysis in experiments was typically less than ~0.8 - 1 L in each of the flume and control tanks. This water was not replaced, except in experiments 4 - 6 (Table DR2) where we added an additional 700 ml of 1:10 tap:de-ionized water to both the flume and control tanks after ~18 days of run time to offset water extraction. In experiments 7, 9, 10, 11, and 14 (Table DR2) we also sampled an additional 1 L of water approximately half way through the experiment for separate analyses, and immediately replaced the sampled water with 1:10 tap:de-ionized water. The dilution factor from water extraction did not exceed ~6%, significantly less than our conservative estimate of 25% error on DOC measurements. For simplicity, we assume error associated with water extraction and addition is subsumed in our estimates of DOC error and do not include error associated with water extraction in our uncertainty estimates of f_{DOC} (Eq. 2).

Initial sediment samples reflecting POC composition at the start of the experiment were collected prior to sediment introduction in the flume and control tanks. We filtered flume and control water through single-use 0.22 μm PES filters at the end of experiments to retrieve sediment. In select cases we allowed sediment to settle for >12 h and decanted a portion of the clear water before either filtering or allowing the remaining water to evaporate in a drying oven between 40-50 $^{\circ}\text{C}$. After collection, sediment was oven-dried between 40-50 $^{\circ}\text{C}$ for >24 h and stored in combusted glass vials.

Dried sediment samples were split into separate aliquots for grain size measurements at the GFZ Sed Lab and geochemical analysis at Durham University. In all experiments aliquots for grain size analysis were placed in a sodium pyrophosphate dispersion agent for >24 h to break down aggregates before running samples through a laser diffraction particle size analyzer (Retsch/Horiba LA950) capable of measuring particles between 0.1 and 2500 μm in 92 logarithmically spaced bins. Counts were converted to volume percent applying the Mie scattering theory with a refraction index of 1.55 and an absorption index of 1.33, and we calculated particle size distribution based on the median of 10 successive measurements. Replicate analysis of select samples showed variation in median grain size (D_{50}) up to ~15%. We conservatively apply 15% uncertainty to all laser diffraction measurements, and propagate this error in estimates of ΔD_{50} (Figure 2A).

Large grain sizes in Experiments 6 and 14 (Table DR3) led to >15% variability in laser diffraction measurements, due in part to the small sample sizes (typically <0.4 g) used for laser diffraction analysis. For all material from Experiment 14 and the starting material and ending material from the control tank in Experiment 6, we instead measured grain size distributions using a Retsch Camsizer XT (Table DR3) which can measure large sample masses (>10g) to capture sample heterogeneity. The Camsizer digitally images grains and measures grain diameter over 297 linearly spaced bins between 30 μm – 3 cm. We use the Camsizer grain diameter estimate based on the equivalent diameter of the area equivalent circle of the particle projection. Replicate analysis of select Camsizer measurements shows D_{50} variability <5%, and we propagate this 5% error in ΔD_{50} calculations (Figure 2A). Significant abrasion in the flume run of Experiment 6 produced fine grains that were below the detection limit of the Camsizer, and we report grain size estimates from laser diffraction measurements for this run (Table DR3).

For select samples, we additionally measured specific surface area (SSA) of sediments using a Micromeritics Gemini VII gas sorption analyzer. We measured the molar amount of nitrogen gas (N_2) adsorbed to the total particle surface area in 1-2 grams of bulk sample material under increasing gas pressure. For each sample, a linear adsorption isotherm was calculated using measurements at five pressure conditions and specific surface area (m^2/g dry sediment) was determined using the Brunauer, Emmett, and Teller (BET) theory (Brunauer et al., 1938).

Solid sample aliquots (~20 g) for geochemical analyses were powdered in a disc mill and decarbonated following Galy et al (2007). C_{org} and stable carbon isotope measurements were carried out using a Costech Elemental Analyser (EA) coupled via a CONFLO III to a Thermo Scientific Delta V Advantage isotope ratio mass spectrometer (IRMS) at Durham University. Measurements were normalized using internal and international standards and corrected for internal and procedural blanks (Grocke et al., 2011). Stable carbon isotope ratios are reported in

$\delta^{13}\text{C}$ notation relative to Vienna Pee Dee belemnite (VPDB). Isotopic accuracy was monitored through routine analyses of in-house standards, which were stringently calibrated against international standards (e.g., USGS 24, 40, IAEA 600, CH3, CH7): this provided a total linear range in $\delta^{13}\text{C}$ between -46‰ and $+3\text{‰}$. Analytical uncertainty in $\delta^{13}\text{C}$ was typically $\pm 0.1\text{‰}$ or better for replicate analyses of the international standards. Total organic carbon was obtained as part of the isotopic analysis using an internal standard (Glutamic Acid, 40.82‰C). Error on calculating C_{org} using replicate analyses of the internal standard and duplicate analyses is on the order of 3% of the measured value. We propagate 3% error on C_{org} in all ΔM_c calculations.

The concentration of Re in solid samples was determined with 300 to 500 mg of powdered sample in a volume of 3 mL HF 27N and 3 mL of HNO_3 16N in PTFE beakers heated at 120°C for at least 24 h. After digestion, samples were evaporated until dry at 80°C and then re-dissolved in aqua regia in order to destroy fluorides and heated at 120°C for 24 h before being re-evaporated again. Finally, samples were re-dissolved in HCl (concentration $\sim 1\text{N}$). For samples containing refractory organic matter, the solid black residue was treated in concentrated HNO_3 16N and aqua regia for several days at temperature of 160°C in order to oxidize a maximum amount of organic matter. Rhenium was then separated from the rest of the matrix using an ion-chromatography chemical procedure modified from previously described methods (Miller et al., 2009; Chu et al., 2015). Polypropylene columns with an inner diameter of the bed area of 7.1 mm were filled with 1 mL of AG1-X8 resin (200-400 mesh) which was cleaned (30 mL of HNO_3 8N) and conditioned (5 mL of HCl 1N) before introduction in a HCl 1M medium. Before eluting the Re, elution of the rest of the matrix was done in 3 steps: (1) matrix cleaning by adding 10 mL of HCl 1N, (2) addition of 15 mL of HNO_3 0.5N, and (3) 1.5 mL of HNO_3 4N. Re was eluted with 12.5 mL of HNO_3 4N. After elution, the Re eluted fraction was evaporated at $100\text{--}120^\circ\text{C}$ until completely dry. Re was re-taken into solution and concentration was measured by direct calibration as per water samples (described above).

5. Changes in water temperature, pH, and dissolved oxygen

For our experiments, flume water temperatures were typically near $24\pm 3^\circ\text{C}$, and motor heat caused flumes to run $\sim 3^\circ\text{C}$ higher than their corresponding static control tanks (Table DR5). Water pH started at ~ 7.5 and typically remained between 7 and 8.5, (with the exception of the lignite experiment where values decreased to ~ 5 to 4) (Table DR5). Except for a single outlier, dissolved oxygen levels in flume experiments always exceeded 95%. Dissolved oxygen in control experiments was typically above 90%, with the exception of the lignite experiment where values progressively decreased from $\sim 98\%$ to 55% (Table DR5).

6. Quantifying solid phase POC loss

Calculation of ΔM_c (Eq. 1) requires estimates of the initial and final carbon mass. We estimate $M_{c_initial}$ as

$$M_{c_initial} = \frac{C_{org_initial}}{100} \times M_{sed} \quad , \quad (\text{DR4})$$

where $C_{org_initial}$ and M_{sed} are the initial POC concentration (wt. %) and experiment sediment mass, respectively. To calculate M_{c_final} we correct the POC concentration measured at the end of the experiment (C_{org_final} , wt. %) for mass loss to the dissolved phase (M_{diss}) as

$$M_{c_final} = \frac{C_{org_final}}{100} [M_{sed} - M_{diss}] . \quad (DR5)$$

We calculate M_{diss} from the change in TDS and tank water volume (V)

$$M_{diss} = TDS_{final} V_{final} - TDS_{initial} V_{initial} , \quad (DR6)$$

where the subscripts initial and final refer to the start and end of the experiment, respectively.

The main contributors to TDS are Ca^{2+} , SO_4^{2-} and HCO_3^- (Table DR6) indicating carbonate dissolution and sulfide oxidation during the experiments. Mass loss from solids due to DOC production was negligible relative to TDS (Tables DR4 and DR6). Propagating uncertainty from TDS, C_{org} , and V results in ~4% error on ΔM_c measurements, which stem primarily from the 3% uncertainty in C_{org} . Water addition in select experiments (DR Section 3) resulted in TDS changes of up to 2%, less than the up to 7% uncertainty on TDS measurements, and, for simplicity, is not included in M_{diss} uncertainty estimates.

Despite the mass loss correction, three of the control experiments and one of the flume experiments show POC gain (ΔM_c values of $7 \pm 4\%$ and $8 \pm 4\%$, Figure 2b). Gains likely reflect heterogeneity in C_{org} values within samples beyond what is accounted for in the 3% uncertainty. Small amounts of POC-enriched (e.g. macromolecular organic matter) or POC-depleted (mineral grains, quartz) phases could shift the measured C_{org} values. Small gains in POC are consistent with our general finding of less than 10% POC mass loss ($\Delta M_c > -10\%$) during experiments (Figure 2B). Future, more precise measurements of POC loss may benefit from tracking the gaseous products of oxidation such as CO_2 (e.g., Beaupre et al., 2016).

Estimates of f_{DOC} (Eq. 2) use the maximum measured mass of DOC over the experiment (M_{DOC_max}) calculated as

$$M_{DOC_max} = DOC_{max} V_{t_max} - DOC_{initial} V_{initial} , \quad (DR7)$$

where $DOC_{initial}$ and DOC_{max} are the initial and maximum DOC concentrations measured before and after adding sediment to the experiment, respectively, and V_{t_max} is the flume or control tank volume at the time of the maximum DOC concentration, and is estimated from a linear interpolation of $V_{initial}$ and V_{final} (Table DR2). We propagate uncertainty on DOC, V , and $M_{c_initial}$ measurements to estimate f_{DOC} error.

7. Dissolved load geochemistry during POC_{petro} experiments

Shale experiments showed consistent behavior in the evolution of major (Ca^{2+} , SO_4^{2-} , TDS) and trace (Re) dissolved ion concentrations during the experiments. The sediment addition caused a rapid increase in major ion concentrations over a period of ~4 days, followed by a slower increase in concentration during the remaining experiment time (Figure DR4). The lignite experiment showed similar behavior to the shale experiments with initially rapid increase in Re and SO_4^{2-} over the first ~1 day, which slowed with time (Figure DR4). The rapid increase in dissolved concentrations following sediment addition may reflect ion-exchange between fresh sediment and a fluid that is not in equilibrium with that solid (e.g., Sayles and Mangelsdorf, 1979; Lupker et al., 2016), rapid release of solutes from defect sites (White and Brantley, 2003), and/or rapid carbonate weathering (Chou et al., 1989).

Regardless of the exact chemical process that takes place during the first 1-4 days of $\text{POC}_{\text{petro}}$ the experiments, the rapid solute production does not well represent the processes acting in lowland rivers, where sediments have been in contact with water since prior to their erosion (e.g. in the saturated zone) and during erosion, transport and deposition. Here we seek to examine the slower production of solutes that occurs by oxidation and/or acid-hydrolysis reactions (“weathering”) between the fluid and solid that occurs after the initial rapid solute production. To do this, we examine the dissolved Re/SO_4 versus Re/Na ratios over the duration of the experiments. Oxidation of sulfide minerals is expected to outpace $\text{POC}_{\text{petro}}$ oxidation, which in turn outpaces silicate mineral acid hydrolysis (Chang and Berner, 1999). This suggests that weathering reactions should increase SO_4 , Re and Na concentrations over time, but that Re/SO_4 should decrease while Re/Na increases over time. This behavior starts at around 1 and 4 days in the lignite and shale experiments, respectively, and continues for the remaining portion of the experiment (Tables DR2 and DR6, Figure DR5), consistent with a switch from ion-exchange, leaching, or rapid carbonate dissolution to “weathering” reactions. We remove Re produced in this initial period of rapid solute production from our calculation of f_{Re} (Eq. 3) by solving for $M_{\text{diss_Re}}$ as

$$M_{\text{diss_Re}} = \text{Re}_{\text{final}} V_{\text{final}} - \text{Re}_{\text{initial}} V_{\text{initial}} - M_{\text{blank}} \quad (\text{DR8})$$

where Re_{final} is the Re concentration at the end of the experiment and $\text{Re}_{\text{initial}}$ is the Re concentration after 1 and 4 days in the lignite and shale experiments, respectively. M_{blank} is a correction for Re production that occurred in blank experiments (Figure DR2, Tables DR2 and DR6). For flume experiments with $D_{50} > 250 \mu\text{m}$, we set M_{blank} to 60 ng based on the 60 ng increase in rhenium in the blank experiment transporting combusted quartz sediment (which we attribute to abrasion of the stainless steel flume and/or production of Re from inclusions in the silicate mineral). Other $\text{POC}_{\text{petro}}$ experiments had grain sizes below the threshold for viscous dampening and we set $M_{\text{blank}} = 0.3 \text{ ng}$ for flume experiments based on the increase in rhenium in the sediment-free blank experiment. We set $M_{\text{blank}} = 0 \text{ g}$ for all control experiments based on negligible increases in rhenium in control experiments (Table DR6). Finally, we calculate the initial solid load mass of Re as

$$M_{\text{Re_initial}} = \text{Re}_{\text{initial}} \times M_{\text{sed}} \quad (\text{DR9})$$

where $\text{Re}_{\text{initial}}$ is the sediment rhenium concentration at the start of the experiment.

8. Comparison with field estimates of POC loss

We seek to estimate the loss of $\text{POC}_{\text{petro}}$ that occurs between the mountain front and coastline in the Amazon and Gages rivers. Because $\text{POC}_{\text{petro}}$ in these basins is sourced exclusively from the river headwaters, the losses represent the total $\text{POC}_{\text{petro}}$ loss from both in-river fluvial transport and floodplain storage. In the Amazon basin, Bouchez et al. (2010) report a decrease in $C_{\text{org_petro}}$ from $0.26\% \pm 0.11\%$ at the mountain front (the Rio Beni near Rurrenabaque, Bolivia) to $0.02\% \pm 0.03\%$ in the lowland basin (the mouth of the Rio Madeira, Brazil). Using the upper limit of $C_{\text{org_petro}} = 0.37\%$ at the mountain front and the mean value of $C_{\text{org_petro}} = 0.02\%$ in the lowland basin, we estimate an upper bound of 95% $\text{POC}_{\text{petro}}$ loss during lowland river transit. This estimate assumes that $C_{\text{org_petro}}$ is not influenced by sediment input from unconstrained tributaries, which deliver ~60% of the total sediment load (Bouchez et al., 2010). To account for sediment from unconstrained tributaries, we represent $\text{POC}_{\text{petro}}$ concentration measured at the

mouth of the Rio Madeira ($C_{\text{org_petro_Madeira}}$) as a mix of $\text{POC}_{\text{petro}}$ from sediment sourced from the Rio Beni ($C_{\text{org_petro_Beni_source}}$) and unconstrained tributaries ($C_{\text{org_petro_unconstrained_sources}}$), i.e.,

$$C_{\text{org_petro_Madeira}} = 0.4(C_{\text{org_petro_Beni_source}}) + 0.6(C_{\text{org_petro_unconstrained_sources}}) \quad (\text{DR10})$$

Solving Eq. (DR10) for $C_{\text{org_petro_Beni_source}}$ assuming the sediment from unconstrained tributaries is $\text{POC}_{\text{petro}}$ free ($C_{\text{org_petro_unconstrained_sources}} = 0$), and conservatively assuming $C_{\text{org_petro_Madeira}}$ varies between its mean value (0.02%) and its upper limit (0.05%), yields $0.05\% < C_{\text{org_petro_Beni_source}} < 0.125\%$. We thus estimate $C_{\text{org_petro}}$ loss using the lower limit of $C_{\text{org_petro}} = 0.15\%$ measured at the mountain front and the upper limit of $C_{\text{org_petro}} = 0.125\%$ in the lowland basin after 60% dilution from assumed $\text{POC}_{\text{petro}}$ free tributaries. This yields a conservative lower estimate of $\text{POC}_{\text{petro}}$ loss of 17%.

For the Ganges basin, $C_{\text{org_petro}}$ at the mountain front ranges from 0.03-0.07% for the Narayani, Karnali, and Kosi rivers (Galy et al., 2008). These rivers account for ~67% of the total sediment flux to the main stem Ganges, and yield a sediment-flux weighted average value of $C_{\text{org_petro}}=0.05\%$ compared to $C_{\text{org_petro}}=0.025\%$ on the Ganges near its outlet in Bangladesh (Galy et al., 2008; Galy et al., 2015). Using the flux-weighted average $C_{\text{org_petro}}$ value, and assuming the unconstrained tributaries have $0.0 < C_{\text{org_petro}} < 0.05\%$, yields $C_{\text{org_petro}}$ losses of 27-51% from the mountain front to the Ganges in Bangladesh.

In order to compare field measurements with our experiments of ~900-1200 km of suspended sediment transport (Table DR2), we assume $\text{POC}_{\text{petro}}$ losses are linearly proportional to river transport distance. Based on the ~2300 km of transport between the Rio Beni at Rurrenabaque and the mouth of the Rio Madeira we reduce transport losses by a factor of $1000 \text{ km} / 2300 \text{ km} = 0.43$ to yield $C_{\text{org_petro}}$ losses of 7-41% per 1000 km of fluvial transit in the Amazon basin. Transport distances between the mountain front and the lowland Ganges in Bangladesh range from ~550-1000 km for pathways investigated by Galy et al (2008). As the upper limits of these distances approximately match the transport in our flume experiment, we conservatively apply no correction and estimate $\text{POC}_{\text{petro}}$ losses of 27-51% per ~500-1000 km of transport in the Ganges basin.

While the field measurements and flume experiments can be compared using similar transport length scales, they represent timescales that can differ by orders of magnitude. By continuously transporting sediment without floodplain storage, our flume experiments achieved order ~1000 km of suspended sediment transport in ~50 days. In contrast, the residence time of sediment crossing the Amazon basin can be of order ky (Dosseto et al., 2006; Wittmann et al., 2015), due to transient floodplain storage during downstream transit. The negligible POC losses observed in our flume experiments compared to the large losses observed in the Amazon and Ganges basins are consistent with the hypothesis that the majority of POC oxidation occurs during floodplain storage (Torres et al., 2017; Scheingross et al., 2018). Trapping of sediment behind natural and man-made dams may provide an additional source of sediment storage; however, high sedimentation rates in dams is thought to promote POC preservation (Li et al., 2015), rather than oxidation which can occur in shallow floodplain deposits.

9. Pilot experiments

We performed three pilot experiments to aid in designing the experimental protocol. Differences in methods and standards between the pilot and main experiments make comparing the experiment sets difficult; nonetheless we report the pilot experiment methods and data for

archival purposes. Two of the pilot experiments used the same lignite and shale sediment from the main experiments, while the third used organic-rich soil collected within 5 cm of the surface from a temperate forest in Potsdam, Germany. We expect that the soil should be free of $\text{POC}_{\text{petro}}$ due to the combination of high rates of litterfall in the forest and underlying deposits of glacial outwash sands derived largely from Fennoscandian basement rocks

Pilot experiments followed identical methods to the primary experiments discussed in the main text with the exceptions listed here. Pilot experiments used a smaller volume control tank and had different sediment to water ratios than the main experiments (Table DR2). The pilot soil and lignite experiments used exclusively de-ionized water, and the pilot shale experiment used exclusively tap water. In the pilot shale experiment we added fresh sediment to both the flume and control after ~14 days to observe the effect of sediment doubling. In the pilot soil experiment, we dry-sieved 150 g soil to $<125 \mu\text{m}$ and added 50 g of 125-400 μm diameter combusted quartz sand to promote soil comminution. Quartz sand was within the zone of partial viscous damping, limiting its abrasion in the experiment and allowing separation of the quartz and soil at the end of the experiment by sieving to size fractions greater and less than 125 μm , respectively. In pilot experiments with soil and lignite (Table DR2) we progressively added ~2 L of water to the flume over the course of the experiment and ~0.2 – 0.5 L to the control tank to account for evaporative and sample losses.

References:

- Bagnold, R. A., 1966, An approach to the sediment transport problem for general physics: Washington, D.C., US Geological Survey Professional Paper 422-I.
- Beaupre, S. R., Mahmoudi, N., and Pearson, A., 2016, IsoCaRB: A novel bioreactor system to characterize the lability and natural carbon isotopic (C-14, C-13) signatures of microbially respired organic matter: *Limnology and Oceanography-Methods*, v. 14, no. 10, p. 668-681.
- Bouchez, J., Beyssac, O., Galy, V., Gaillardet, J., France-Lanord, C., Maurice, L., and Moreira-Turcq, P., 2010, Oxidation of petrogenic organic carbon in the Amazon floodplain as a source of atmospheric CO_2 : *Geology*, v. 38, no. 3, p. 255-258.
- Brunauer, S., Emmett, P., and Teller, E., 1938, Adsorption of Gases in Multimolecular Layers: *Journal of the American Chemical Society*, v. 60, no. 2, p. 309-319.
- Chang, S. B., and Berner, R. A., 1999, Coal weathering and the geochemical carbon cycle: *Geochimica Et Cosmochimica Acta*, v. 63, no. 19-20, p. 3301-3310.
- Chanson, H., 2004, *Hydraulics of Open Channel Flow*, Amsterdam, Elsevier.
- Chatanantavet, P., Whipple, K. X., Adams, M. A., and Lamb, M. P., 2013, Experimental study on coarse grain saltation dynamics in bedrock channels: *Journal of Geophysical Research-Earth Surface*, v. 118, no. 2, p. 1161-1176.
- Chou, L., Garrels, R. M., and Wollast, R., 1989, Comparative study of the kinetics and mechanisms of dissolution of carbonate minerals: *Chemical Geology*, v. 78, p. 269-282.
- Chu, Z. Y., Yan, Y., Chen, Z., Guo, J. H., Yang, Y. H., Li, C. F., and Zhang, Y. B., 2015, A Comprehensive Method for Precise Determination of Re, Os, Ir, Ru, Pt, Pd Concentrations and Os Isotopic Compositions in Geological Samples: *Geostandards and Geoanalytical Research*, v. 39, no. 2, p. 151-169.
- Dietrich, W. E., 1982, Settling velocity of natural particles: *Water Resources Research*, v. 18, no. 6, p. 1615-1626.
- Dosseto, A., Bourdon, B., Gaillardet, J., Allegre, C. J., and Filizola, N., 2006, Time scale and conditions of weathering under tropical climate: Study of the Amazon basin with U-series: *Geochimica Et Cosmochimica Acta*, v. 70, no. 1, p. 71-89.
- Galy, V., Beyssac, O., France-Lanord, C., and Eglinton, T., 2008, Recycling of Graphite During Himalayan Erosion: A Geological Stabilization of Carbon in the Crust: *Science*, v. 322, no. 5903, p. 943-945.
- Galy, V., Bouchez, J., and France-Lanord, C., 2007, Determination of total organic carbon content and delta C-13 in carbonate-rich detrital sediments: *Geostandards and Geoanalytical Research*, v. 31, no. 3, p. 199-207.
- Galy, V., Peucker-Ehrenbrink, B., and Eglinton, T., 2015, Global carbon export from the terrestrial biosphere controlled by erosion: *Nature*, v. 521, no. 7551, p. 204-207.

- Garcia, M. H., 2008, Sediment transport and morphodynamics, *in* Garcia, M. H., ed., *Sedimentation Engineering: Processes, Measurements, Modeling, and Practice*: Reston, Virginia, American Society of Civil Engineers.
- Grocke, D. R., Hori, R. S., Trabucho-Alexandre, J., Kemp, D. B., and Schwark, L., 2011, An open ocean record of the Toarcian oceanic anoxic event: *Solid Earth*, v. 2, no. 2, p. 245-257.
- Joseph, G. G., Zenit, R., Hunt, M. L., and Rosenwinkel, A. M., 2001, Particle-wall collisions in a viscous fluid: *Journal of Fluid Mechanics*, v. 433, p. 329-346.
- Li, G., Wang, X. C. T., Yang, Z. F., Mao, C. P., West, A. J., and Ji, J. F., 2015, Dam-triggered organic carbon sequestration makes the Changjiang (Yangtze) river basin (China) a significant carbon sink: *Journal of Geophysical Research-Biogeosciences*, v. 120, no. 1, p. 39-53.
- Lupker, M., France-Lanord, C., and Lartiges, B., 2016, Impact of sediment-seawater cation exchange on Himalayan chemical weathering fluxes: *Earth Surface Dynamics*, v. 4, no. 3, p. 675-684.
- McLean, S. R., 1992, On the calculation of suspended-load for noncohesive sediments: *Journal of Geophysical Research-Oceans*, v. 97, no. C4, p. 5759-5770.
- Miller, C. A., Peucker-Ehrenbrink, B., and Ball, L., 2009, Precise determination of rhenium isotope composition by multi-collector inductively-coupled plasma mass spectrometry: *Journal of Analytical Atomic Spectrometry*, v. 24, no. 8, p. 1069-1078.
- Rohl, H. J., Schmid-Rohl, A., Oschmann, W., Frimmel, A., and Schwark, L., 2001, The Posidonia Shale (Lower Toarcian) of SW-Germany: an oxygen-depleted ecosystem controlled by sea level and palaeoclimate (vol 165, pg 27, 2001): *Palaeogeography Palaeoclimatology Palaeoecology*, v. 169, no. 3-4, p. 271-+.
- Sayles, F. L., and Mangelsdorf, P. C., 1979, Cation-Exchange Characteristics of Amazon River Suspended Sediment and Its Reaction with Seawater: *Geochimica Et Cosmochimica Acta*, v. 43, no. 5, p. 767-779.
- Scheingross, J. S., Brun, F., Lo, D. Y., Omerdin, K., and Lamb, M. P., 2014, Experimental evidence for fluvial bedrock incision by suspended and bedload sediment: *Geology*, v. 42, no. 6, p. 523-526.
- Scheingross, J. S., Repasch, M., Hovius, N., Sachse, D., Dellinger, M., Lupker, M., Hilton, R. G., Eglinton, T., Grocke, D., Golombek, N., and Orfeo, O., 2018, The fate of organic carbon during lowland river transport and transient floodplain storage: AGU Fall Meeting abstract V11E-0070.
- Schreck, P., and Glasser, W., 1998, Regional geology of the lignite mining districts in eastern Germany: *Acidic Mining Lakes*, p. 15-21.
- Schuessler, J. A., Kampf, H., Koch, U., and Alawi, M., 2016, Earthquake impact on iron isotope signatures recorded in mineral spring water: *Journal of Geophysical Research-Solid Earth*, v. 121, no. 12, p. 8548-8568.
- Sklar, L. S., and Dietrich, W. E., 2004, A mechanistic model for river incision into bedrock by saltating bed load: *Water Resources Research*, v. 40, no. 6.
- Smith, J. C., 2013, Particulate organic carbon mobilisation and export from temperate forested uplands [PhD: University of Cambridge].
- Torres, M. A., Limaye, A. B., Ganti, V., Lamb, M. P., West, A. J., and Fischer, W. W., 2017, Model predictions of long-lived storage of organic carbon in river deposits: *Earth Surface Dynamics*, v. 5, no. 4, p. 711-730.
- White, A. F., and Brantley, S. L., 2003, The effect of time on the weathering of silicate minerals: why do weathering rates differ in the laboratory and field?: *Chemical Geology*, v. 202, no. 3-4, p. 479-506.
- Wittmann, H., von Blanckenburg, F., Dannhaus, N., Bouchez, J., Gaillardet, J., Guyot, J. L., Maurice, L., Roig, H., Filizola, N., and Christl, M., 2015, A test of the cosmogenic Be-10(meteoric)/Be-9 proxy for simultaneously determining basin- wide erosion rates, denudation rates, and the degree of weathering in the Amazon basin: *Journal of Geophysical Research-Earth Surface*, v. 120, no. 12, p. 2498-2528.

Data Repository Tables (see separate excel file)

Table DR1: Flow velocity measurements

Table DR2: Summary of experiments

Table DR3: Summary of solid load carbon, rhenium, and granulometry measurements

Table DR4: Results of liquid-chromatography organic carbon detection (LC-OCD) measurements

Table DR5: Multiprobe measurements of flume and control tank water

Table DR6: Inorganic dissolved load measurements

Table DR7: Uncertainty estimates of dissolved load measurements

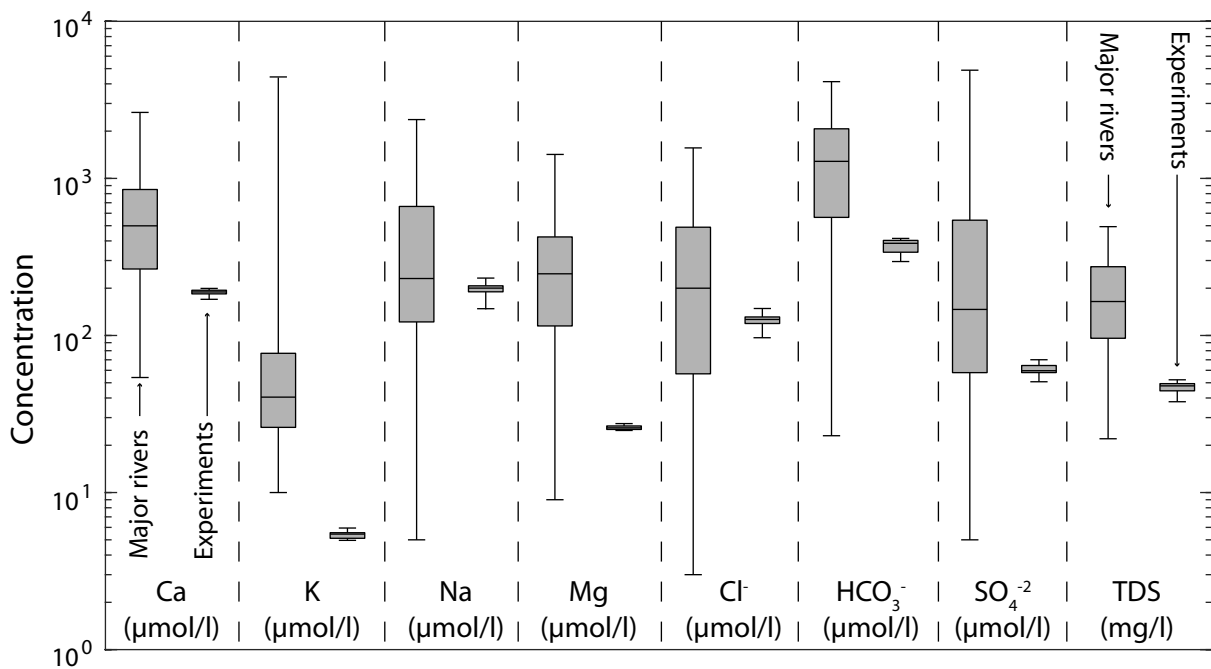


Figure DR1: Comparison of dissolved chemistry from major rivers (Gaillardet et al., 1999) (left box plots) versus starting composition of water used in experiments (right box plots). Box and whisker plots show data median, interquartile range, and data extent. Following Gaillardet et al. (1999), we excluded rivers with total dissolved solids (TDS) >500 mg/l based on likely anthropogenic influence.

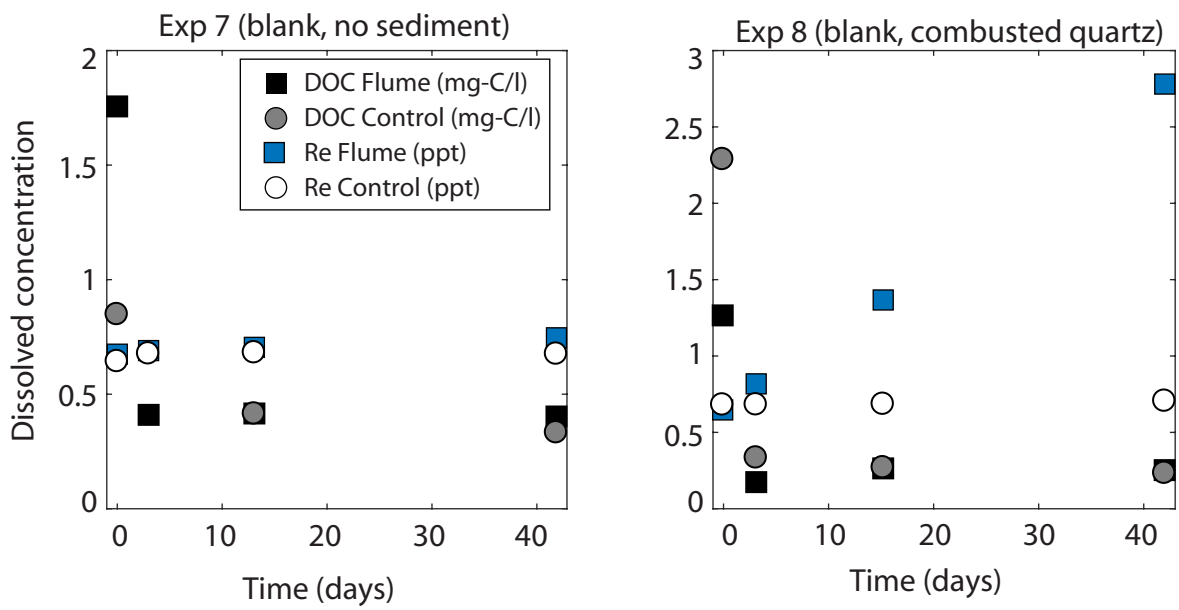


Figure DR2: Evolution of dissolved organic carbon (DOC) and Re concentrations in blank experiments.

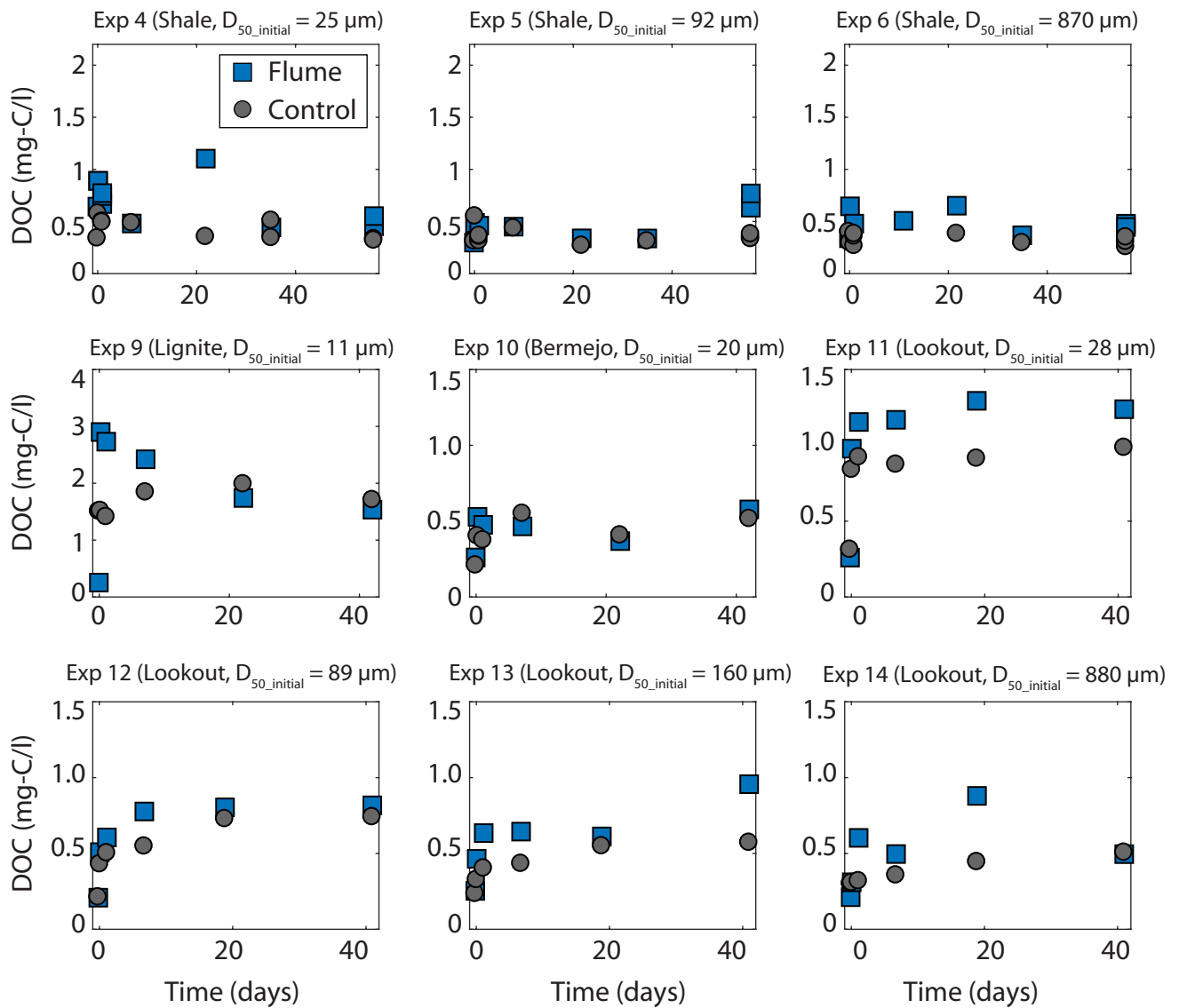


Figure DR3: Evolution of dissolved organic carbon (DOC) concentration during flume and control experiments. $D_{50_initial}$ is the median grain diameter at the start of the experiment.

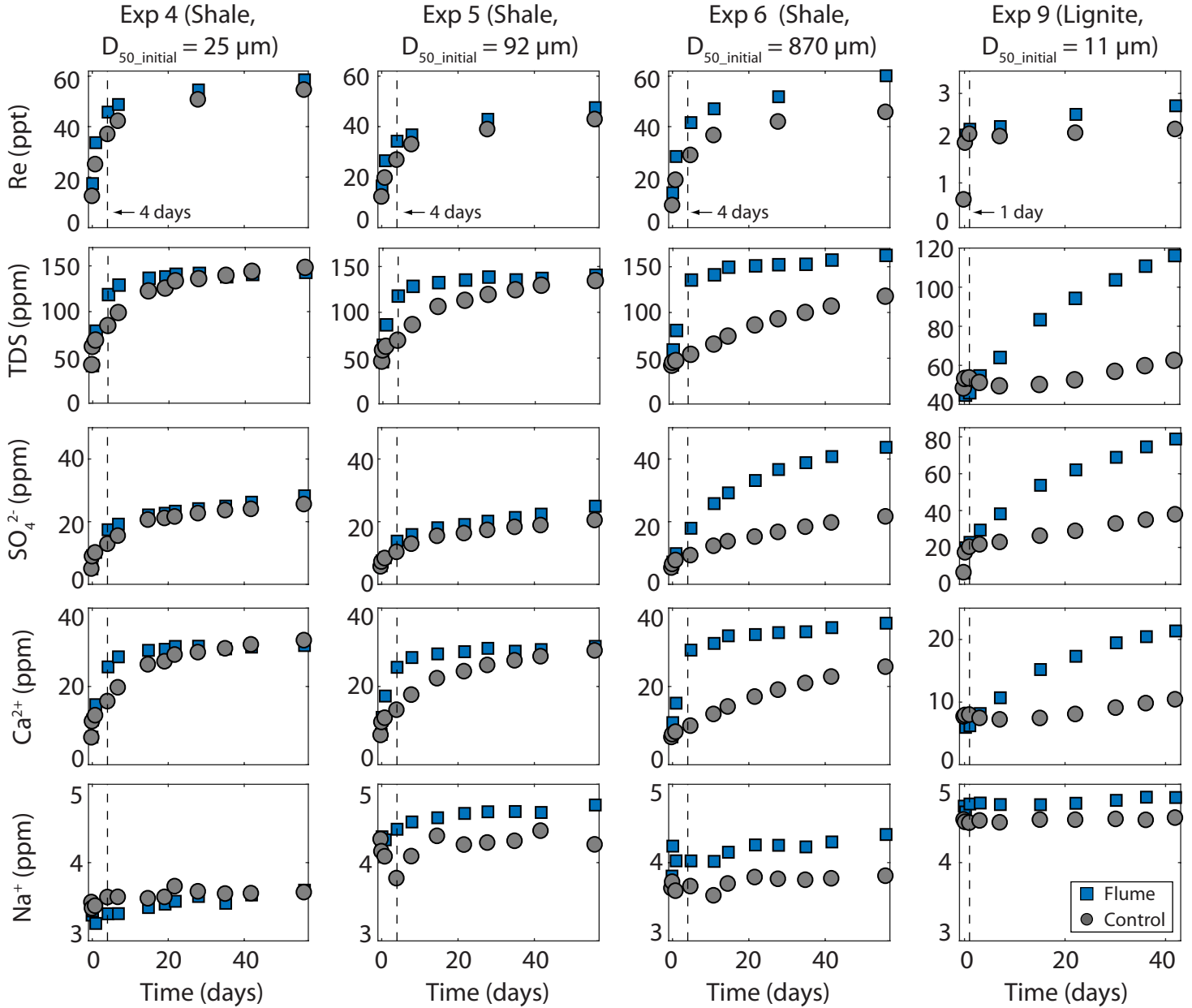


Figure DR4: Evolution of dissolved rhenium, total dissolved solids (TDS), SO_4^{2-} , Ca^{2+} , and Na^+ for $\text{POC}_{\text{petro}}$ experiments. Dashed lines show the transition from rapid solute production inconsistent with lowland rivers to inferred oxidative weathering. $D_{50_initial}$ is the grain diameter at the start of the experiment.

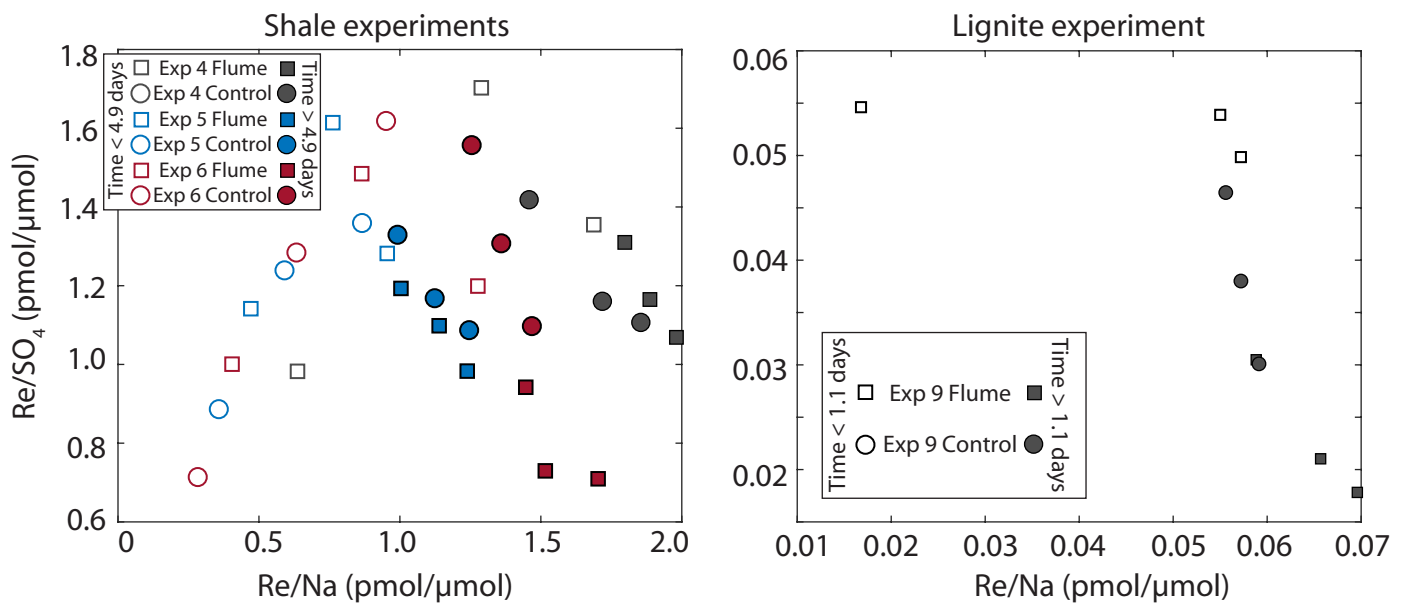


Figure DR5: Re/SO_4 vs Re/Na for shale and lignite experiments. Open symbols are periods of rapid solute production and closed symbols are periods of inferred oxidative weathering.